Influence of the spacer on the photoreactivity of flurbiprofen-tyrosine dyads

Ignacio Vayá,[a]* Thomas Gustavsson,[b] Dimitra Markovitsi,[b] Miguel A. Miranda,[a] and M. Consuelo Jiménez[a]*

[a] Departamento de Química/Instituto de Tecnología Química UPV-CSIC, Universitat Politècnica de València, Camino de Vera s/n, 46022 Valencia, Spain, E-mail: mcjimene@qim.upv.es, igvapre@qim.upv.es

[b] LIDYL, Laboratoire Interactions, Dynamiques et Lasers, CEA, CNRS, Université Paris-Saclay, CEA Saclay, 91191 Gif-sur-Yvette, France

Abstract

The photoreactivity of diastereomeric dyads containing (*S*)- or (*R*)-flurbiprofen (FBP) and (*S*)-Tyr, either directly linked (**1**) or separated by a cyclic spacer (**3**) has been investigated. The main feature is a remarkable intramolecular quenching of FBP fluorescence, especially in **1**. The process is clearly configuration dependent, being more efficient for the (*R,S*)- diastereomer in **1** and for the (*S,S*)- analogue in **3**. Noteworthy, exciplex emission is detected in the 380-500 nm region in the case of **3**. Fluorescence decay kinetics from the femtosecond to the nanosecond time-domains provides evidence for the dynamic nature of the quenching. In agreement with the steady-state and time-resolved observations, molecular modelling points to a more favourable geometric arrangement of the two interacting chromophores in **1** than in **3**.

Keywords: Exciplex, Fluorescence Quenching, Fluorescence Upconversion, Laser Flash Photolysis, Time-correlated Single Photon Counting

1. Introduction

The binding of drugs to proteins constitutes an active research field in connection with drug transport and distribution through the organism, which is ultimately related to the therapeutic action. The interactions existing between drugs and proteins can modulate properties of the former, such as solubility in plasma, susceptibility to some reagents or in vivo half-life [1-4]. In this context, a better knowledge on the drug/protein complexation process can shed light on the structural bases leading to the design of new therapeutic agents [5, 6].

Transport proteins, such as serum albumins, are in charge of the binding and transport of endogenous and exogenous target molecules through the blood stream [7]. Human serum albumin (HSA) contains 585 amino acid residues, one Trp, 17 disulfide bridges, and one free Cys [8, 9]. Small organic molecules usually bind to HSA in the so-called site I and site II, following Sudlow's classification [10]; the only Trp residue is located in site I, while site II is mainly made-up of Tyr, His and Arg [7]. The role played by different amino acids when drugs are incorporated within the protein cavities has been widely investigated, especially for Tyr and Trp, which have become universal fluorescent markers for protein studies[11-15]. In addition, it is known that chemical modifications on these amino acids result in a decrease of drugs affinity for the protein [16, 17]. For instance, the presence of a Tyr residue influences the esterase activity of bovine serum albumin (BSA) [18].
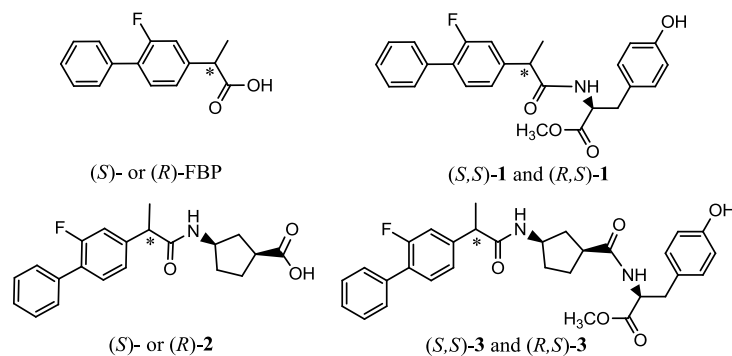
Flurbiprofen (FBP, Scheme 1) is a nonsteroidal anti-inflammatory drug (NSAID) prescribed for treatment of osteoarthritis, rheumatoid arthritis, tendinitis, bursitis, sunburns and prevention of migraine headache [19-24]. Although it is prescribed as a racemic mixture, its pharmacological effect is attributed to the (*S*)- enantiomer [25, 26]. Its photobehaviour has been characterised either in aqueous or organic media [27], and binding to HSA has been investigated by spectroscopic techniques, namely fluorescence and laser flash photolysis [28-31]. Upon FBP complexation, a dynamic fluorescence quenching of ^{1}FBP* and ^{1}Trp* is observed, due to energy and electron transfer processes [29]. Concerning ^{3}FBP*, the triplet lifetime (τ_T) lengthens within the protein cavities, as a result of the protection provided by the microenvironment that prevents

from attack by oxygen [28, 30, 31]. Enantioselectivity has been observed in the photobehaviour of (*R*)- and (*S*)-FBP/HSA complexes [29, 30, 32].

The use of dyads that contain a drug covalently linked to an amino acid is a useful tool to mimic processes that occur in the protein binding sites of the real supramolecular complexes. In this context, light-induced events such as energy transfer, electron transfer, or exciplex formation on drug-amino acid dyads have provided the key to demonstrate the mechanistic pathways responsible for photoallergy or to estimate the preferred binging site in HSA[29, 33-37].

We have recently reported a thorough photophysical study on FBP/HSA mixtures, comparing their photobehaviour with that of FBP-Trp dyads [29]; stereoselective dynamic fluorescence quenching has been noticed in the model systems, although the kinetics of the involved processes are slower than in the real drug/protein complexes. Interestingly, an inversed stereodifferentiation has been noticed in the dyads with respect to that found for FBP@HSA complexes; this can be explained because the relative conformations of the FBP and Trp moieties are not necessarily the same in the dyads and within the protein.

In order to improve the picture on FBP/HSA interactions in the excited states, here we describe the photobehaviour of a series of diastereomeric dyads composed of FBP and Tyr, a fluorescent close-lying amino acid that may also influence the binding process. The design envisages the two subunits either directly linked or separated by means of a rigid spacer (Scheme 1). A comparative study on the different dyads would provide useful information on how the distance and conformational arrangement between the chromophores may affect the photophysical properties.

Scheme 1. Chemical structures of the investigated systems.

2. Experimental section

2.1. Materials and methods

(S)- and (R)-Flurbiprofen, (S)-tyrosine methyl ester hydrochloride (TyrMe), (1S,3R)-3-amino-cyclopentanecarboxylic acid, 1-hydroxybenzotriazole (BtOH), N,N'-dicyclohexylcarbodiimide (DCC), N-hydroxysuccinimide (NHS) and 1-(3-dimethylaminopropyl)-N-ethylcarbodiimide hydrochloride (EDC) were purchased from Sigma-Aldrich. Their purity was checked by ^{1}H NMR and HPLC analysis. Spectrophotometric HPLC or reagent grade solvents were obtained from Scharlab and used without further purification. The ^{1}H-NMR and ^{13}C-NMR spectra were recorded in CDCl$_3$ at 400 and 100 MHz, respectively, using a Bruker AVANCE III instrument; chemical shifts are reported in ppm. Steady state absorption spectra were recorded in a JASCO V-630 spectrophotometer. The X-ray structure was determined at Unidade de Raios X, at the Universidade de Santiago de Compostela. Crystallographic data (excluding structure factors) for the (R,S)-**1** structure have been deposited at the Cambridge Crystallographic Data Centre as supplementary publication number CCDC 662961.

Exact mass values were obtained using an Ultra Performance Liquid Chromatography (UPLC) ACQUITY UPLC system (Waters Corp.) with a conditioned autosampler at 4 °C. The separation was accomplished on an ACQUITY UPLC BEH C18 column (50 mm × 2.1 mm i.d., 1.7 μm), which was maintained at 40 °C. The analysis was performed using acetonitrile and

water (80:20 v/v containing 0.01% formic acid) as the mobile phase with a flow rate of 0.5 mL/min and an injection volume of 5μL. The Waters ACQUITY™ XevoQToF Spectrometer (Waters Corp.) was connected to the UPLC system via an electrospray ionization interface. This source was operated in positive ionization mode at 100 °C with the capillary voltage at 1.5 kV and a temperature of desolvation of 300 °C. The cone and desolvation gas flows were 40 and 800 L/h, respectively. The collision gas flow and collision energy applied were 0.2 mL/min and 12 V, respectively. All data collected in Centroid mode were acquired using Masslynx™ software (Waters Corp.). Leucine-enkephalin was used at a concentration of 500 pg/μL as the lock mass generating an $[M+H]^+$ ion (m/z 556.2771) and fragment at m/z 120.0813 with a flow rate of 50 μL/min to ensure accuracy during the MS analysis.

Steady-state fluorescence spectra were obtained using a JASCO spectrofluorometer system provided with a monochromator in the wavelength range 200-900 nm, with an excitation wavelength of 267 nm at 22 ºC. Solutions were placed into 10 mm × 10 mm quartz cells. The absorbance of the samples at the excitation wavelength was kept below 0.1. Fluorescence quantum yields were determined using FBP in MeCN as reference, with $\phi_F = 0.17$ (air) or $\phi_F = 0.21$ (N_2) [27].

2.2. Equipment

Time-resolved fluorescence measurements were performed using the fluorescence upconversion (FU) and time-correlated single photon counting (TCSPC) techniques. The excitation source was the third harmonic (267 nm) of a mode-locked Ti-Sapphire laser, delivering ~120 fs pulses whose repetition rate was 76 and 4.75 MHz for FU and TCSPC, respectively (in the latter case set by a pulse-picker).

For the FU measurements, a home-built setup was used. This has been described in detail earlier [38, 39]. Briefly, a 1 mm type I BBO sum-frequency crystal was used, providing an instrumental response function of about 350 fs (fwhm). We judge that the time resolution of the setup is better than 100 fs after deconvolution, depending on the signal-to-noise ratio. The

average excitation power used was 40 mW. The power density cannot be measured precisely within the excitation volume but we estimate it to 0.2 ± 0.1 GW/cm^2 for a 40 mW output from the tripler unit (assuming a 40 micron diameter of the focused beam). Solutions (about 30 mL) were kept flowing through a 0.4 mm quartz cell, which was kept in continuous motion perpendicular to the excitation beam in order to minimize thermal effects.

For the TCSPC experiments, a Becker & Hickl GmbH SP-630 PC card was used [40]. The fluorescence from a standard quartz cell was collected and focused onto the entrance slit of a small monochromator (Jobin-Yvon HR250) using off-axis parabolic mirrors. In order to cut the laser light, a Schott WG 295 filter was placed in front of the slit. Moreover, a Glan-Thompson polarizer ensured that only the vertical component of the fluorescence was detected. The detector was a microchannel plate (R1564 U Hamamatsu) providing an instrumental response function of 60 ps (fwhm). The average laser power (0.1 mW at 4.75 MHz) was measured with a Melles Griot broadband powermeter. The irradiated area on the surface of the cell was ca. 0.2 cm^2 corresponding to a pulse intensity of 2.4 kW/cm^2. Solutions were contained in a 10 mm $\times$ 10 mm quartz cell and continuously stirred. Successive recordings with the same sample gave identical decays, which were eventually merged to improve the signal-to-noise ratio. Such a procedure allowed us to ensure that the measured signals were not altered during the measurements due to a possible accumulation of photoproducts.

The time-resolved experiments were performed either at magic angle or under successive parallel ($I_{par}(t)$) and perpendicular ($I_{perp}(t)$) excitation/detection conditions. For both FU and TCSPC, the polarization of the exciting beam was set to be either vertical or horizontal using a zero-order half-wave plate. Since only the vertical component of the emission was detected, in FU by the phase matching conditions of the crystal and in TCPSC by placing a Glan-Thomson polarizer in front pf the monochromatic, the parallel and perpendicular components are defined only by the polarization of the excitation beam. From the measurements of the parallel and perpendicular components, the total (magic angle) fluorescence and the fluorescence anisotropy were calculated from the formulae:

$$F(t) = I_{par}(t) - GI_{perp}(t) \tag{1}$$

$$r(t) = \frac{I_{par}(t) - GI_{perp}(t)}{I_{par}(t) + 2GI_{perp}(t)} \tag{2}$$

The transmission under parallel and perpendicular conditions was found to be identical so the correction factor *G* was put to unity.

To evaluate the characteristic times involved, instead of treating F(t) and r(t) separately we performed a merged nonlinear fitting/deconvolution process using the impulse response model functions

$$i_{par}(t) = (1 + 2r(t))f(t) \tag{1a}$$

$$i_{perp}(t) = (1 - r(t))f(t) \tag{1b}$$

convoluted by the Gaussian instrument response function, $I(t) \propto i(t) \otimes G(t)$. The model functions thus obtained were fitted to the experimentally measured (I_{par}) and (I_{perp}) signals. The full width at half maximum (fwhm) value of a Gaussian apparatus function was found to be about 375 ± 12 fs fwhm at 330 nm.

Laser flash photolysis (LFP) experiments were performed with a Q-switched Nd:YAG laser (Quantel Brilliant, 266, 4 mJ per pulse, 5 ns fwhm) coupled to a mLFP-111 Luzchem miniaturised equipment. This transient absorption spectrometer includes a ceramic xenon light source, 125 mm monochromator, Tektronix 9-bit digitizer TDS-3000 series with 300 MHz bandwidth, compact photomultiplier and power supply, cell holder and fibre optic connectors, fibre optic sensor for laser-sensing pretrigger signal, computer interfaces, and a software package developed in the LabVIEW environment from National Instruments. The LFP equipment supplies 5 V trigger pulses with programmable frequency and delay. The rise time of the detector/digitizer is ~3 ns up to 300 MHz (2.5 GHz sampling). The monitoring beam is provided by a ceramic xenon lamp and delivered through fibre optic cables. The laser pulse is

probed by a fibre that synchronizes the LFP system with the digitizer operating in the pretrigger mode. Transient spectra were recorded employing 10 mm × 10 mm quartz cells with 4 mL capacity and were bubbled for 15 min with N_2 before acquisition. The concentration of FBP in MeCN was 2.5×10^{-5} M. The experiments were carried out at room temperature.
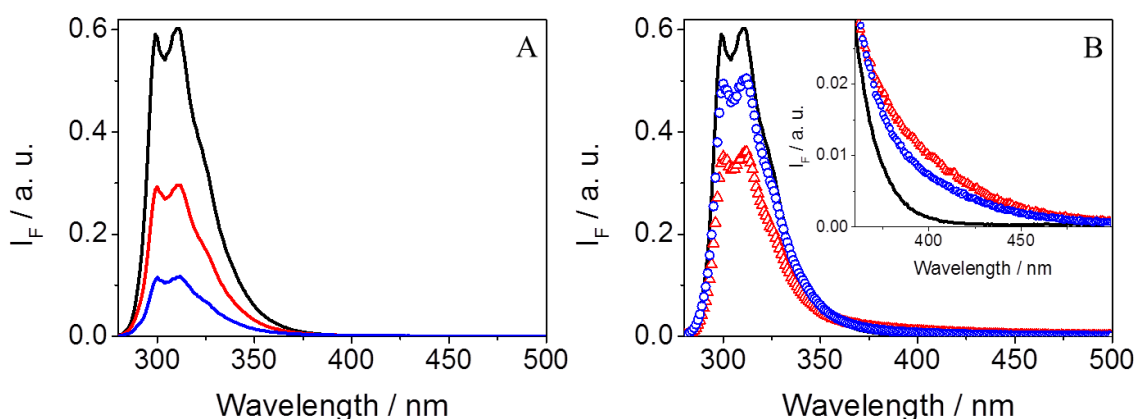
3. Results and discussion

Diastereomeric dyads (*S,S*)- and (*R,S*)-**1** (containing (*S*)- or (*R*)-FBP and (*S*)-TyrMe directly linked) and (*S,S*)- and (*R,S*)-**3** (with the two subunits separated by a rigid spacer) were synthesised by conventional methods. The synthesis and chemical characterization of the new compounds are shown in detail in the SI. Briefly, for **1**, direct coupling of FBP and TyrMe was performed in the presence of EDC and BtOH; for compounds **3**, the drug was initially reacted to the cyclic spacer in the presence of DCC and DMAP, leading to **2**; the latter was esterified with TyrMe, to afford the final products. We were able to obtain crystals of (*R,S*)-**1**, its X-ray structure is presented in the supplementary data (Fig. S7 in the SI).

Due to the poor solubility of the dyads in aqueous media, the experiments were performed in acetonitrile. The UV absorption spectra of dyads **1** and **3** were identical to the added spectra of the isolated components (FBP+TyrMe or **2**+TyrMe, respectively) at the same concentration (see Fig. S8 in the SI); this indicates no significant ground-state interaction between the two partners. The presence of the cyclic spacer did not affect the photophysical properties of FBP; thus, the photobehaviour of the dyads was always compared to that of FBP.
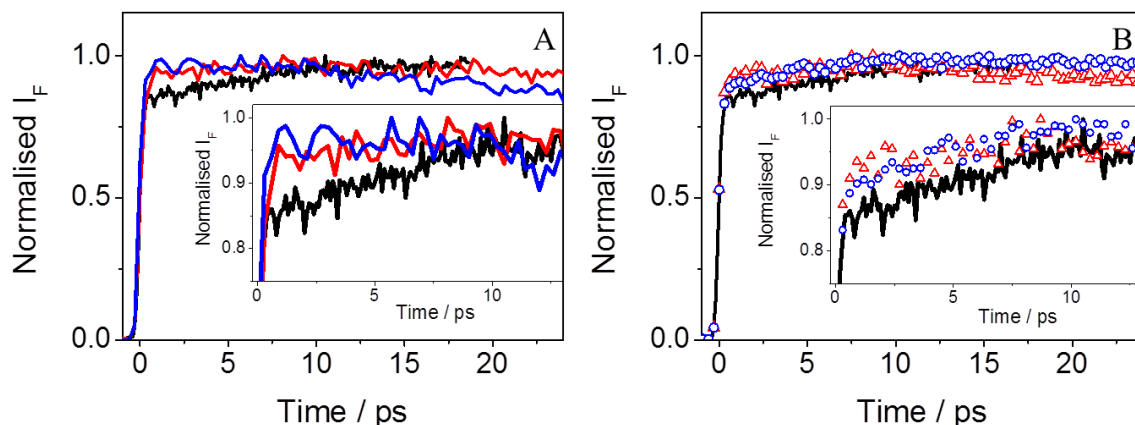
Steady-state fluorescence spectra of isoabsorptive solutions ($A_{267} = 0.1$) of **1**, **3** and FBP were recorded at $\lambda_{exc} = 267$ nm; at this wavelength, *ca*. 90% of the photons are absorbed by FBP. The emission consisted on the typical FBP band with maximum at 310 nm, in agreement with the lower singlet excited state energy of FBP (99 kcal/mol) compared to that of Tyr (100 kcal/mol) [27, 41]. Interestingly, quenching of ^{1}FBP* was observed for all the dyads, being more efficient for **1** than for **3** (compare Fig. 1A and 1B). The process was stereoselective, with stronger quenching for (*R,S*)-**1** than for (*S,S*)-**1** (Fig. 1A); the opposite trend was found for **3**: here, the

(*S*,*S*)-diastereomer evidenced higher quenching than its (*R*,*S*)- analogue (Fig. 1B). Remarkably, a tiny but not negligible emission tail was detected for **3** at longer wavelengths (>350 nm), with intensity slightly higher for (*S*,*S*)-**3**. This fluorescence can be assigned to exciplex species [42-44], which should normally emit at lower energies and was not observed in the case of dyads **1**. Actually, subtraction of the normalised emission of FBP from that of normalised emission of dyads **3** clearly evidenced the fluorescence arising from exciplexes, with λ_{max} ca. 360 nm (see Fig. S9 in the SI).
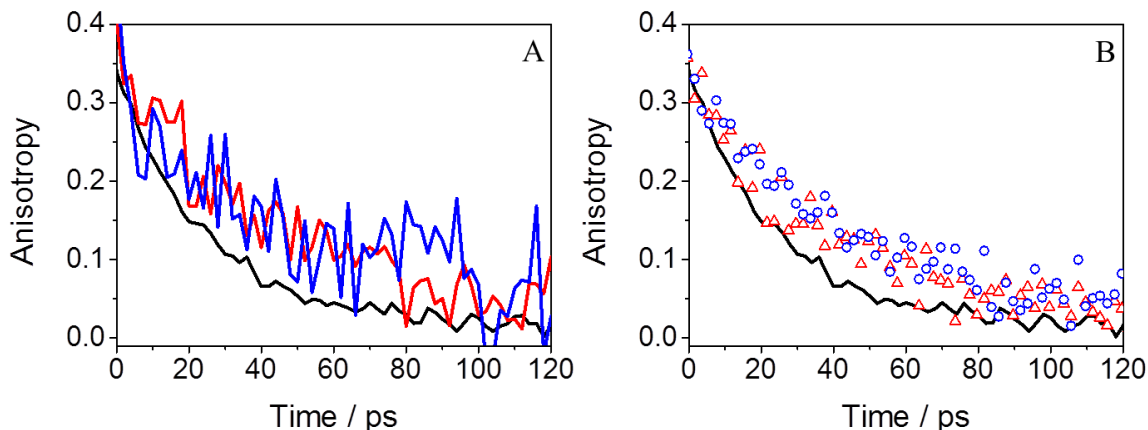

Fig. 1. Fluorescence spectra of A) (*S*)-FBP (black line), (*S*,*S*)-**1** (red line) and (*R*,*S*)-**1** (blue line), and B) (*S*)-FBP (black line), (*S*,*S*)-**3** (red triangles) and (*R*,*S*)-**3** (blue circles) after excitation at 267 nm in deaerated MeCN. The inset shows emission from exciplex states for dyads **3**.

In order to investigate the dynamic behaviour, femtosecond fluorescence upconversion (FU) measurements were performed after excitation at 267 nm (Fig. 2). As observed in a previous report, a rise of 7.0 ± 0.6 ps was detected for FBP, assigned to a vibrational relaxation in the excited state [45]. A similar rise was also detected for **3**, although less pronounced than in FBP (see Fig. 2B). However, instantaneous [1]FBP* formation was noticed for (*S*,*S*)-**1** and (*R*,*S*)-**1** (Fig. 2A); this can be caused by a stronger drug/amino acid coupling. After 10 ps, the kinetic profile of (*R*,*S*)-**1** started to decay faster than that of the (*S*,*S*)- analogue; this trend was still observed at longer time-scales (see Fig. S10 in the SI). Dyads **3** showed an opposite behaviour.

Fig. 2. Normalised FU decays at λ_{mon} = 310 nm for A) (*S*)-FBP (black line), (*S,S*)-**1** (red line) and (*R,S*)-**1** (blue line), and B) (*S*)-FBP (black line), (*S,S*)-**3** (red triangles) and (*R,S*)-**3** (blue circles) after excitation at 267 nm in MeCN. The insets show a zoom of the decay traces.

As explained above, the fluorescence anisotropies at 310 nm were calculated from the parallel and perpendicular traces of FBP, **1** and **3** recorded by FU (λ_{exc} = 267 nm) at 310 nm. The fluorescence anisotropies are shown in Fig. 3. The fitting curves obtained for the parallel and perpendicular decay traces are shown in Fig. S11 in the SI. The anisotropy decays were longer for the dyads than for the parent drug. The fluorescence anisotropy of FBP decayed with a characteristic time of about 25 ± 1 ps, with a zero time fluorescence anisotropy r_0 = 0.34 ± 0.02. However, the anisotropy decays of (*S,S*)-**1** and (*R,S*)-**1** were 51 ± 3 ps (r_0 = 0.36 ± 0.02) and 54 ± 4 ps (r_0 = 0.36 ± 0.02), respectively. Similar results were obtained for (*S,S*)-**3** (50 ± 3 ps; r_0 = 0.36 ± 0.02) and (*R,S*)-**3** (52 ± 4 ps; r_0 = 0.33 ± 0.02). The high r_0 values for all dyads indicate that the emission comes from the directly excited state, with no change in their electronic nature. Besides, the longer characteristic times for the dyads compared to monomeric FBP are in full agreement with their larger hydrodynamic volumes. The absence of any fast anisotropy decay at early times, together with the mono-exponential behaviour of the kinetics, point to the lack of internal rotation between the two chromophores at this time-scale.
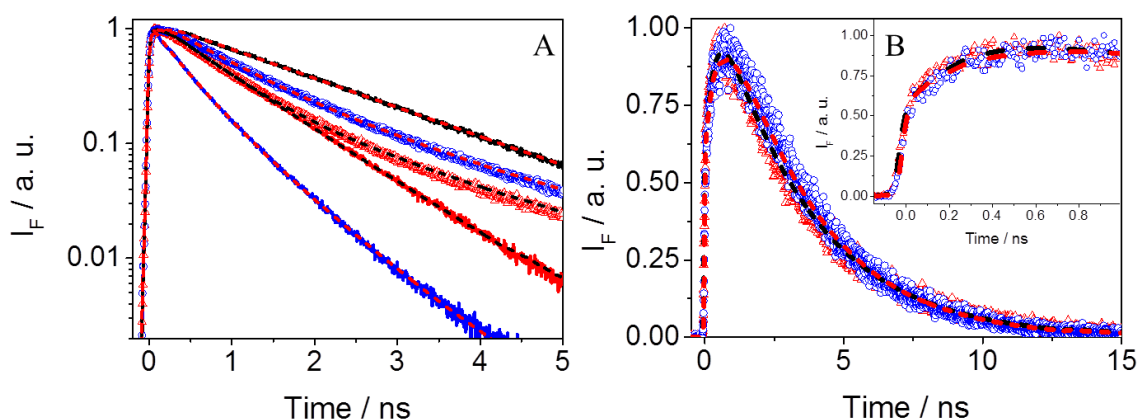
Fig. 3. FU anisotropy decays at λ_{mon} = 310 nm for A) (*S*)-FBP (black line), (*S,S*)-**1** (red line) and (*R,S*)-**1** (blue line), and B) (*S*)-FBP (black line), (*S,S*)-**3** (red triangles) and (*R,S*)-**3** (blue circles) after excitation at 267 nm in aerated MeCN.

To fully characterize the dynamics of the investigated systems, time-correlated single photon counting (TCSPC) measurements in the nanosecond range were performed. The fluorescence of the dyads decayed much faster than that of the isolated drug at 310 nm, indicating an efficient dynamic quenching of ^{1}FBP* (see Fig. 4A). This quenching is clearly stereoselective. Interestingly, the decay of (*R,S*)-**1** was faster than that of the (*S,S*)- analogue; by contrast, the opposite trend was observed for **3**, in agreement with the steady-state and FU data. The decay of FBP followed a monoexponential law, while two lifetime components were necessary to get a good fitting in the dyads; this can be assigned to different conformations. For calculation of rate constants and quantum yields, the average lifetime $<\tau_F>$ was employed in all cases (see Table 1).

The quenching rate constants (k_Q), determined from the fluorescence lifetimes ($<\tau_F>$) were on the order of 10^8-10^9 s^{-1}, with higher values for dyads **1** than for **3**. As regards the radiative rate constants (k_F), obtained from τ_F and ϕ_F, they were found to be in the range of 10^8 s^{-1}. These results are in agreement with the steady-state measurements.

In the case of **3**, the kinetic profiles at 420 nm (Fig. 4B) decayed much slower than those at 310 nm. Interestingly, these kinetics were characterised by a rapid rise of 0.38 ± 0.01 ns and 0.69 ±

11

0.01 ns for (*S,S*)-**3** and (*R,S*)-**3**, respectively; this can be attributed to the formation of the exciplex [29, 46], previously detected in the steady-state measurements. The exciplex lifetimes were 3.27 ± 0.01 ns and 3.05 ± 0.01 ns for (*S,S*)- and (*R,S*)-**3**, respectively. Indeed, the anisotropy decay traces at 420 nm were found to be zero at all times for both diastereomers (see Fig. S12 in the SI), contrary to that recorded at 310nm. This points to a completely different nature of the electronically excited state emitting at 420 nm compared to that emitting at 310 nm. This strengthens our assignment of the long wavelength emission to an exciplex state for which a radical change in emission dipole direction can be expected.

Fig. 4. Normalised TCSPC decays (λ_{exc} = 267 nm, MeCN) at A) λ_{mon} = 310 nm for (*S*)-FBP (black line), (*S,S*)-**1** (red line), (*R,S*)-**1** (blue line), (*S,S*)-**3** (red triangles) and (*R,S*)-**3** (blue circles) (fitted curves are shown in dash) or B) λ_{mon} = 420 nm for (*S,S*)-**3** (red triangles) and (*R,S*)-**3** (blue circles). The inset shows the kinetic rise of the traces monitored at 420 nm during the first nanosecond. Fitted curves: black dash for (*S,S*)-**3** and red dash for (*R,S*)-**3**.

Table 1. Photophysical parameters for FBP and dyads **1** and **3** in MeCN.[a] The fluorescence lifetimes were measured by TCSPC.

	FBP	(*S,S*)-**1**	(*R,S*)-**1**	(*S,S*)-**3**	(*R,S*)-**3**
ϕ_F	0.17	0.09	0.04	0.11	0.15
$<\tau_F>$ (ns)[b]	1.67	0.90	0.36	0.93	1.20
k_F ($\times 10^{-8}$ s^{-1})[c]	1.02	1.00	1.10	1.18	1.25
k_Q ($\times 10^{-9}$ s^{-1})[d]		0.51	2.17	0.48	0.24
$\phi_{Q(dyn)}$[e]		0.46	0.79	0.44	0.28
ϕ_T[f]	0.71	0.27	0.14	0.22	0.39

[a] The absorbance of the samples was 0.1 at λ_{exc} = 267 nm;[b] $<\tau_F>$ = $a_1\tau_1$+ $a_2\tau_2$, λ_{mon} = 310 nm;[c] $k_F = \phi_F/\tau_F$;[d] k_Q = $(1/\tau_F(dyad)$ -$1/\tau_F(FBP))$;[e] $\phi_Q(dyn) = \phi_F(dyad)k_Q(dyad)/k_F(dyad)$;[f] $\phi_T = \phi_T(FBP)\Delta A(dyad)/\Delta A(FBP)$.

It is known that exciplexes exhibit partial charge separation [47], which is consistent with the electron donating character of Tyr [11]. In fact, fluorescence quenching could be due to electron transfer (ET) or exciplex formation (EXC). Application of the Weller equation allowed us to estimate the ΔG values corresponding to the two possible pathways (equations 3 and 4) [41, 48, 49]:
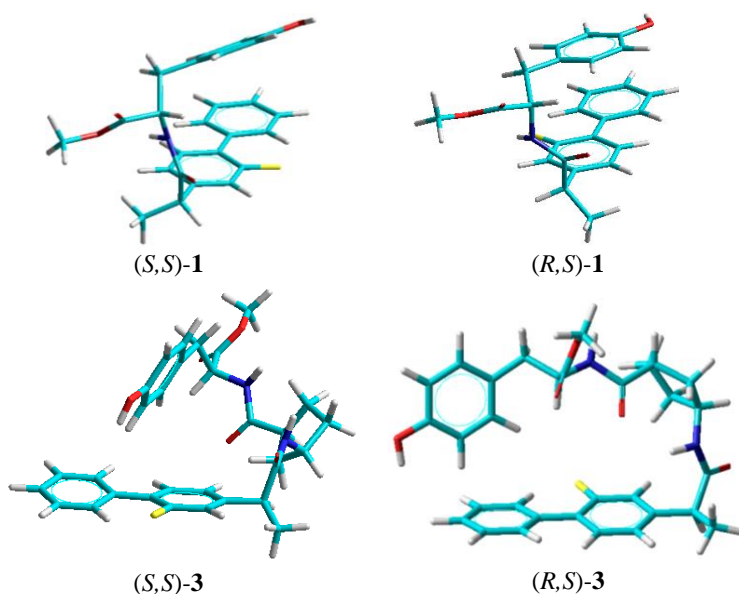
$$\Delta G_{ET} = E_{OX} - E_{RED} - \frac{E_{0-0}}{23.061} + \frac{2.6}{\varepsilon} - 0.13 \tag{3}$$

$$\Delta G_{EXC} = E_{OX} - E_{RED} - \frac{E_{0-0}}{23.061} - \frac{\mu^2}{\rho^3}\left(\frac{\varepsilon-1}{2\varepsilon+1} - 0.19\right) + 0.38 \tag{4}$$

where E_{OX} and E_{RED} are the redox potentials of the involved chromophores [50], E_{0-0} is the energy of ^{1}FBP* (99 kcal mol^{-1}) [27], ε is the dielectric constant of the solvent (37.5 for MeCN), and μ^2/ρ^3 has a constant value of 0.75 eV. After considering all these parameters, both processes were found to be exergonic, with ΔG_{ET} = -9 kcal mol^{-1} and ΔG_{EXC} = -4 kcal mol^{-1}. Indeed, the exciplex was directly observed in dyads **3**.

In order to clarify the differences in the stereoselective fluorescence quenching of the dyads, and to get more insight into the conformational arrangements of the two chromophores in the linked systems, simple molecular modelling (PM3) was performed (Fig. 5). The geometrical arrangement of FBP and Tyr was favoured for interaction in (*R,S*)-**1** due to its folded
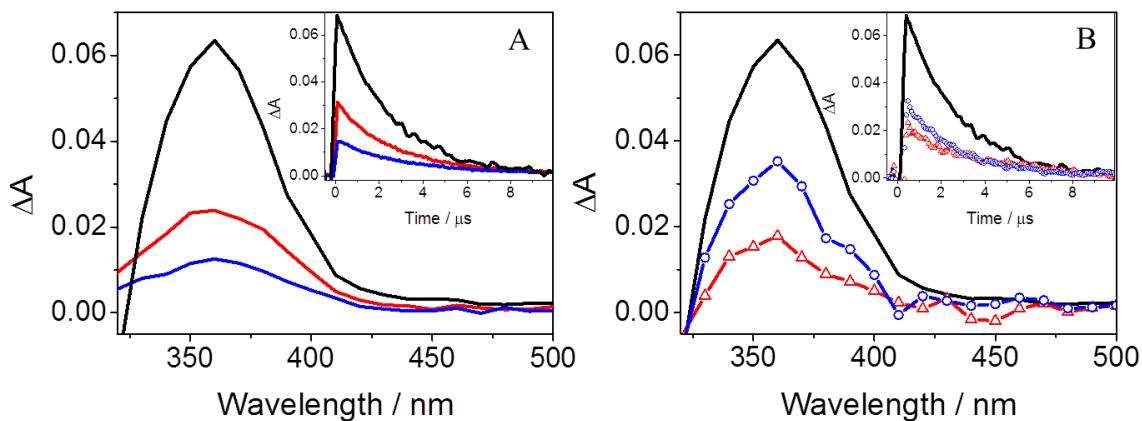
conformation, which also prevails in the solid state (see Fig. S7 in the SI); this matches with its higher fluorescence quenching compared to (*S*,*S*)-**1**, whose geometry was more distorted and consequently the quenching was lower. Concerning dyads **3**, they clearly presented a more unfavourable geometry arrangement to interact, which was even more marked for the (*R*,*S*)-diastereomer; here, the two chromophores are practically in orthogonal arrangement, which is in line with its lower fluorescence quenching compared to (*S*,*S*)-**3**.

(*S*,*S*)-**1**   (*R*,*S*)-**1**

(*S*,*S*)-**3**   (*R*,*S*)-**3**

Fig. 5. Geometry optimised (HyperChem Release 8.0.3 for Windows Molecular Model System, PM3) structures for all investigated dyads.

For investigating the excited state dynamics of longer lived transient species, LFP experiments were performed upon excitation at 266 nm, in deaerated acetonitrile. The transient absorption spectra of FBP, **1** and **3** are shown in Fig. 6. The dyads displayed the same absorption band (λ_{max} = 360 nm) as the isolated drug, which was assigned to ^{3}FBP* [27]. The ΔA_{max} value at 360 nm was lower for the dyads than for FBP. This can be explained as a result of the intramolecular quenching of the precursor ^{1}FBP*, and reproduces the observed stereodifferentiation in the singlet excited state. Therefore, for dyads **1**, the (*R*,*S*)-diastereomer displayed the lower ΔA_{max}, while for **3** the same was true for the (*S*,*S*)- analogue. With respect to the triplet lifetime values, they were found to be very similar to that of isolated FBP, evidencing no dynamic quenching of

14

the triplet excited state (see insets in Fig. 6). Indeed, the lack of interactions from the triplet state is in agreement with the Weller equations (3 and 4); thus, considering an energy transfer and/or exciplex formation process from ^{3}FBP* (65 kcal mol^{-1}) [27], it is observed that both processes would be thermodynamically disfavoured, with ΔG_{ET} = +23 kcal mol^{-1} and ΔG_{EXC} = +30 kcal mol^{-1}.

Fig. 6. Laser flash photolysis spectra obtained 0.5 μs after the laser pulse of A) (*S*)-FBP (black line), (*S,S*)-**1** (red line) and (*R,S*)-**1** (blue line), and B) (*S*)-FBP (black line), (*S,S*)-**3** (red triangles) and (*R,S*)-**3** (blue circles) after excitation at 266 nm in deaerated MeCN. The insets show the decay traces at 360 nm.

4. Conclusions

The photophysical properties of diastereomeric dyads composed of flurbiprofen linked to tyrosine, an amino acid residue that plays a key role in the interactions of drugs to transport proteins, have been characterised in detail. The photoreactivity is strongly influenced by the distance and conformational arrangement between the two chromophores. Thus, the directly linked dyads exhibit a more efficient fluorescence quenching than those separated by the cyclic spacer. This stereoselective quenching has been found to be mainly dynamic in nature, as observed from the FU and TCSPC experiments. Application of the Weller equation is in agreement with electron transfer and exciplex formation as the thermodynamically favourable

15

routes for [1]FBP* quenching. Molecular modelling results are in agreement with the detected stereoselectivity. Finally, no significant interactions involving the FBP excited triplet state have been noticed; this observation contrasts with the dramatic lengthening of the triplet lifetimes of the drug within the protein binding sites, which has to be attributed to the microenvironment provided by the tertiary structure of these biomolecules.

Acknowledgements

References

[1] U. Kragh-Hansen, V.T. Chuang, M. Otagiri, Practical aspects of the ligand-binding and enzymatic properties of human serum albumin, Biol. Pharm. Bull., 25 (2002) 695-704.

[2] T. Peters, Serum albumin, in: Advances in Protein Chemistry, Academic Press, New York, 1985, pp. 161-245.

[3] S. Sugio, A. Kashima, S. Mochizuki, M. Noda, K. Kobayashi, Crystal structure of human serum albumin at 2.5 A resolution, Protein Eng., 12 (1999) 439-446.

[4] T. Wybranowski, M. Cyrankiewicz, B. Ziomkowska, S. Kruszewski, The HSA affinity of warfarin and flurbiprofen determined by fluorescence anisotropy measurements of camptothecin, Biosystems, 94 (2008) 258-262.

[5] K. Vuignier, J. Schappler, J.-L. Veuthey, P.-A. Carrupt, S. Martel, Drug-protein binding: a critical review of analytical tools, Anal. Bioanal. Chem, 398 (2010) 53-66.

[6] N.Z. Xie, Q.S. Du, J.X. Li, R.B. Huang, Exploring strong interactions in proteins with quantum chemistry and examples of their applications in drug design, PloS One, 10 (2015) e0137113.

[7] T. Peters, Ligand binding by albumin, in: Elsevier (Ed.) All About Albumin - Biochemistry, Genetics, and Medical Applications, Academic Press, San Diego, 1995, pp. 76-132.

[8] D.C. Carter, J.X. Ho, Structure of serum albumin, in: Advances in Protein Chemistry, Academic Press, New York, 1994, pp. 153-203.

[9] D.L. Schonfeld, R.B. Ravelli, U. Mueller, A. Skerra, The 1.8-A crystal structure of alpha1-acid glycoprotein (Orosomucoid) solved by UV RIP reveals the broad drug-binding activity of this human plasma lipocalin, J. Mol. Biol., 384 (2008) 393-405.

[10] G. Sudlow, D.J. Birkett, D.N. Wade, Further characterization of specific drug binding sites on human serum albumin, Mol. Pharmacol., 12 (1976) 1052-1061.

[11] J.R. Lakowicz, Principles of Fluorescence Spectroscopy, 3rd ed., Plenum Press, New York, 2006.

[12] T. Madrakian, H. Bagheri, A. Afkhami, M. Soleimani, Spectroscopic and molecular docking techniques study of the interaction between oxymetholone and human serum albumin, J. Lumin., 155 (2014) 218-225.

[13] M. Noronha, R. Santos, E. Paci, H. Santos, A.L. Maçanita, Fluorescence lifetimes of tyrosine residues in cytochrome c″ as local probes to study protein unfolding, J. Phys. Chem. B, 113 (2009) 4466-4474.

[14] C. Qin, M.-X. Xie, Y. Liu, Characterization of the myricetin-human serum albumin complex by spectroscopic and molecular modelling approaches, Biomacromolecules, 8 (2007) 2182-2189.

[15] A. Sułkowska, M. Maciążek-Jurczyk, B. Bojko, J. Równicka, W.W. Sułkowski, 1HNMR study of methotrexate-serum albumin (MTX-SA) binding in rheumatoid arthritis, J. Mol. Struct., 891 (2008) 278-283.

[16] J.K. Kamal, L. Zhao, A.H. Zewail, Ultrafast hydration dynamics in protein unfolding: human serum albumin, Proc. Natl. Acad. Sci. U. S. A., 101 (2004) 13411-13416.

[17] A. Sytnik, I. Litvinyuk, Energy transfer to a proton-transfer fluorescence probe: Tryptophan to a flavonol in human serum albumin, Proc. Natl. Acad. Sci. U. S. A., 93 (1996) 12959-12963.

[18] Y. Sakurai, S.F. Ma, H. Watanabe, N. Yamaotsu, S. Hirono, Y. Kurono, U. Kragh-Hansen, M. Otagiri, Esterase-like activity of serum albumin: characterization of its structural chemistry using p-nitrophenyl esters as substrates, Pharm. Res., 21 (2004) 285-292.

[19] P.L. Lomen, L.F. Turner, K.R. Lamborn, M.A. Winblad, R.L. Sack, E.L. Brinn, Flurbiprofen in the treatment of acute gout. A comparison with indomethacin, Am. J. Med., 80 (1986) 134-139.

[20] P. Tan, F.P. Flowers, O.E. Araujo, P. Doering, Effect of topically applied flurbiprofen on ultraviolet induced erythema, Drug Intel. Clin. Pharm., 20 (1986) 496-499.

[21] G.D. Solomon, R.S. Kunkel, Flurbiprofen in the prophylaxis of migraine, Cleveland Clin. J. Med., 60 (1993) 43-48.

[22] R.A. Moore, M.R. Tramer, D. Carroll, P.J. Wiffen, H.J. Mcquay, Quantitive systematic review of topically applied non-steroidal anti-inflammatory drugs, Br. Med. J., 316 (1998) 333-338.

[23] J. Stamp, V. Rhind, I. Haslock, A comparison of nefopam and flurbiprofen in the treatment of osteoarthrosis, Br. J. Clin. Pract., 43 (1989) 24-26.

[24] J. Rovensky, D. Micekova, Six-month prospective study to monitor the treatment of rheumatic diseases with sustained release flurbiprofen, Drug Exp. Clin. Res., 26 (2000) 19-24.

[25] H.-A. Bae, K.W. Lee, Y.-H. Lee, Enantioselective properties of extracellular lipase from Serratia marcescens ES-2 for kinetic resolution of (S)-flurbiprofen, J. Mol. Catal. B-Enzym, 40 (2006) 24-29.

[26] S. Sagdinc, H. Pir, Spectroscopic and DFT studies of flurbiprofen as dimer and its Cu(II) and Hg(II) complexes, Spectrochim. Acta A, 73 (2009) 181-194.

[27] M.C. Jiménez, M.A. Miranda, R. Tormos, I. Vayá, Characterisation of the lowest singlet and triplet excited states of S-flurbiprofen, Photochem. Photobiol. Sci., 3 (2004) 1038-1041.

[28] R. Pérez-Ruiz, C.J. Bueno, M.C. Jimenez, M.A. Miranda, In situ transient absorption spectroscopy to assess competition between serum albumin and alpha-1-acid glycoprotein for drug transport, J. Phys. Chem. Lett., 1 (2010) 829-833.

[29] I. Vayá, P. Bonancia, M.C. Jimenez, D. Markovitsi, T. Gustavsson, M.A. Miranda, Excited state interactions between flurbiprofen and tryptophan in drug–protein complexes and in model dyads. Fluorescence studies from the femtosecond to the nanosecond time domains, Phys. Chem. Chem. Phys., 15 (2013) 4727-4734.

[30] I. Vayá, C.J. Bueno, M.C. Jimenez, M.A. Miranda, Use of triplet excited states for the study of drug binding to human and bovine serum albumins, ChemMedChem, 1 (2006) 1015-1020.

[31] I. Vayá, V. Lhiaubet-Vallet, M.C. Jimenez, M.A. Miranda, Photoactive assemblies of organic compounds and biomolecules: drug-protein supramolecular systems, Chem. Soc. Rev., 43 (2014) 4102-4122.

[32] I. Lammers, V. Lhiaubet-Vallet, M. Consuelo Jimenez, F. Ariese, M.A. Miranda, C. Gooijer, Stereoselective binding of flurbiprofen enantiomers and their methyl esters to human serum albumin studied by time-resolved phosphorescence, Chirality, 24 (2012) 840-846.

[33] N.E. Polyakov, V.K. Khan, M.B. Taraban, T.V. Leshina, O.A. Luzina, N.F. Salakhutdinov, G.A. Tolstikov, Mechanisms of photoinduced electron transfer reactions of lappaconitine with aromatic amino acids. Time-resolved CIDNP study, Org. Biomol. Chem., 3 (2005) 881-885.

[34] I. Vayá, I. Andreu, M.C. Jimenez, M.A. Miranda, Photooxygenation mechanisms in naproxen–amino acid linked systems, Photochem. Photobiol. Sci., 13 (2014) 224-230.

[35] I. Vaya, I. Andreu, V.T. Monje, M.C. Jimenez, M.A. Miranda, Mechanistic studies on the photoallergy mediated by fenofibric acid: photoreactivity with serum albumins, Chem. Res. Toxicol., 29 (2016) 40-46.

[36] I. Vayá, M.C. Jimenez, M.A. Miranda, Excited-state interactions in flurbiprofen-tryptophan dyads, J. Phys. Chem. B, 111 (2007) 9363-9371.

[37] I. Vayá, R. Perez-Ruiz, V. Lhiaubet-Vallet, M.C. Jimenez, M.A. Miranda, Drug-protein interactions assessed by fluorescence measurements in the real complexes and in model dyads, Chem. Phys. Lett., 486 (2010) 147-153.

[38] T. Gustavsson, A. Sharonov, D. Markovitsi, Thymine, thymidine and thymidine 5′-monophosphate studied by femtosecond fluorescence upconversion spectroscopy, Chem. Phys. Lett., 351 (2002) 195-200.

[39] F.-A. Miannay, T. Gustavsson, A. Banyasz, D. Markovitsi, Excited-state dynamics of dGMP measured by steady-state and femtosecond fluorescence spectroscopy, J. Phys. Chem. A, 114 (2010) 3256-2363.

[40] D. Markovitsi, D. Onidas, F. Talbot, S. Marguet, T. Gustavsson, E. Lazzarotto, UVB/UVC induced processes in model DNA helices studied by time-resolved spectroscopy: Pitfalls and tricks, J. Photochem. Photobiol. A, 183 (2006) 1-8.

[41] S.L. Murov, I. Carmichael, G.L. Hug, Handbook of Photochemistry, 2nd ed., Marcel Dekker, 1993.

[42] Y. Wang, O. Haze, J.P. Dinnocenzo, S. Farid, Bonded exciplexes. A new concept in photochemical reactions, J. Org. Chem., 72 (2007) 6970-6981.

[43] Y. Aoki, N. Matsuki, T. Mori, H. Ikeda, Y. Inoue, Exciplex ensemble modulated by excitation mode in intramolecular charge-transfer dyad: effects of temperature, solvent polarity, and wavelength on photochemistry and photophysics of tethered naphthalene-dicyanoethene system, Org. Lett., 16 (2014) 4888-4891.

[44] D.M. Guldi, M. Maggini, G. Scorrano, M. Prato, Intramolecular electron transfer in fullerene/ferrocene based donor-bridge-acceptor dyads, J. Am. Chem. Soc., 119 (1997) 974-980.

[45] P. Bonancia, I. Vayá, M.J. Climent, T. Gustavsson, D. Markovitsi, M.C. Jimenez, M.A. Miranda, Excited-state interactions in diastereomeric flurbiprofen-thymine dyads, J. Phys. Chem. A, 116 (2012) 8807-8814.

[46] T.B. Truong, A. Petit, Charge transfer to solvent state. 4. Luminescence of phenol and tyrosine in different aqueous solvents at 300 and 77 K, J. Phys. Chem., 83 (1979) 1300-1305.

[47] H. Lemmetyinen, N. Tkachenko, A. Efimov, M. Niemi, Transient states in photoinduced electron transfer reactions of porphyrin- and phthalocyanine-fullerene dyads, J. Porphyrins Phthalocyanines, 13 (2009) 1090-1097.

[48] J. Pérez-Prieto, F. Bosca, R. Galian, A. Lahoz, L.R. Domingo, M.A. Miranda, Photoreaction between 2-Benzoylthiophene and Phenol or Indole, J. Org. Chem., 68 (2003) 5104-5113.

[49] A.Z. Weller, Photoinduced electron transfer in solution: exciplex and radical ion pair formation free enthalpies and their solvent dependence, Phys. Chem., 133 (1982) 93-98.

[50] The values of ΔG for the different processes were determined using the equations given in Ref. 49, taken from refs. 41 and 48: E_{OX} = 1.4 V (phenol) and E_{RED} = -2.5 V (biphenyl).